This is an open access article published under an ACS AuthorChoice License, which permits copying and redistribution of the article or any adaptations for non-commercial purposes.

JACS
JOURNAL OF THE AMERICAN CHEMICAL SOCIETY
Article
pubs.acs.org/JACS

How Does Confinement Change Ligand–Receptor Binding Equilibrium? Protein Binding in Nanopores and Nanochannels

Mario Tagliazucchi[†,‡] and Igal Szleifer*[,†]

[†]Department of Biomedical Engineering, Department of Chemistry and Chemistry of Life Processes Institute, Northwestern University, Evanston, Illinois 60208, United States

[‡]INQUIMAE-CONICET, Ciudad Universitaria, Pabellón 2, Ciudad Autónoma de Buenos Aires C1428EHA, Argentina

Supporting Information

ABSTRACT: We present systematic studies for the binding of small model proteins to ligands attached to the inner walls of long nanochannels and short nanopores by polymeric tethers. Binding of proteins to specific ligands inside nanometric channels and pores leads to changes in their ionic conductance, which have been exploited in sensors that quantify the concentration of the proteins in solution. The theoretical predictions presented in this work are aimed to provide a fundamental understanding of protein binding under geometrically confined environments and to guide the design of this kind of nanochannel-based sensors. The theory predicts that the fraction of the channel volume filled by bound proteins is a nonmonotonic function of the channel radius, the length of the tethers, the surface density of the ligands and the size of the proteins. Notably, increasing the density of ligands, decreasing the size of the channel or increasing the size of the protein may lead to a decrease of the fraction of the channel volume filled by bound proteins. These results are explained from the incomplete binding of proteins to the ligands due to repulsive protein–protein and protein–ligand steric interactions. Our work suggests strategies to optimize the change in conductance due to protein binding, for example: (i) proteins much smaller than the radius of the channel may effectively block the channel if tethers of appropriate length are used, and (ii) a large decrease in conductance upon protein binding can be achieved if the channel and the protein are oppositely charged.

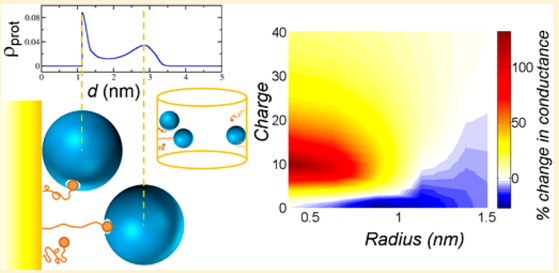

INTRODUCTION

Solid-state nanopores and nanochannels are promising platforms for analytical and bioanalytical devices. In these systems, the presence and concentration of an analyte in solution are determined from changes in the ionic conductance of the channel. There are two main sensing strategies. In the first sensing method, the conductance of a single pore is continuously measured in the presence of an applied potential that drives the translocation of the analyte through the pore. The stochastic translocation events of the analyte give rise to transient changes in conductance, known as resistive pulses, and the concentration of the analyte is determined from the frequency of these pulses.[1−4] In the second sensing strategy, the steady-state conductance of a single nanochannel or an array of nanochannels is measured before and after addition of the analyte. Binding of the analyte to specific ligands on the inner walls of the channel results in changes in the channel conductance that depend on the concentration of the analyte in solution.[5−7] The first strategy (observation of single stochastic translocation events) has received much attention in recent years due to the possibility of extracting information about the translocating molecule, such as the sequence of DNA or RNA chains, from the shape and duration of the resistive pulse. There exists extensive theoretical and simulation work on the translocation of polymers, polyelectrolytes and nanoparticles through pores and channels and the underlying physics is relatively well understood.[8,9] The second strategy, changes in conductance due to specific binding, is a promising technology because it can be implemented in nanopore arrays[7,10,11] and mesoporous materials,[11,12] thereby avoiding the need of single-pore membranes. Moreover, this strategy displays high (bio)chemical specificity because it uses ligands that are specific for the analyte of interest.[5−7,13−17] However, the molecular basis of this strategy remains largely unexplored. Reaching such fundamental knowledge requires the understanding of the competition among physical interactions, molecular organization and ligand–receptor chemical equilibria in confined environments. In the present work, we use a molecular theory to systematically study the binding of proteins to specific ligands lining the inner walls of long nanochannels and short nanopores.

Ligand–receptor binding within a nanochannel affects ionic conductance by a combination of two mechanisms:[14,18,19] (i) a decrease in the volume available for ion transport due to volume exclusion by the bound species and (ii) changes in the concentration of mobile ions within the channel due to the electrostatic charges introduced by the bound species. Examples

Received: May 14, 2015
Published: September 14, 2015

 © 2015 American Chemical Society

DOI: 10.1021/jacs.5b05032
J. Am. Chem. Soc. 2015, 137, 12539−12551

exploiting these mechanisms have been developed to sense proteins,[5−7,14−16,20] DNA,[13,21−24] small organic molecules[11,17,25,26] and metal ions[12,15,27−29] in solution. Martin and co-workers first demonstrated this strategy by studying different ligand−receptor systems in gold-coated conical nanochannels.[5,24] Karnik et al. studied the binding of streptavidin to biotin-modified nanochannels as a function of ionic strength and showed that the resulting ionic current is dictated by the combination of the two mechanisms described above.[14]

Figure 1 shows a schematic representation of the system under study in the present work. We consider nanochannels

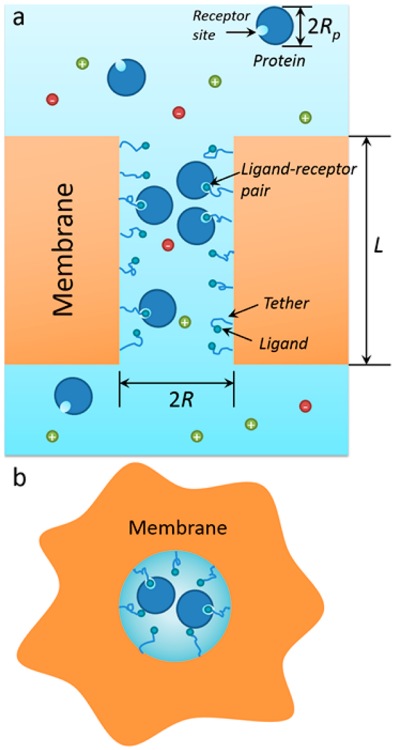

Figure 1. Schematic representation of the system under study along a plane parallel (a) and perpendicular (b) to the channel main axis. The inner walls of a cylindrical nanopore or nanochannel of radius R and length L are coated with ligands that specifically bind to proteins in solution. The ligands have a surface density σ and are connected to the channel walls by flexible polymeric tethers of N segments. The solution contains water molecules, cations, anions, protons, hydroxyl ions and unbound proteins, which can freely rotate and translate. Each protein is modeled as a sphere of radius R_{prot} and charge Q_{prot}, which have only one receptor site for the ligands on its surface.

(radius much smaller than length) or nanopores (radius and length of similar dimensions) whose inner walls are coated with ligands specific for the proteins in solution. In many experimental studies the ligands are linked to the channel walls either by polymeric or oligomeric tethers[6,10] or by long molecular spacers.[13,14] Therefore, we consider in this work spacer tethers of different length connecting the ligands to the channel walls. The use of long and flexible spacers is motivated by experimental[30−32] and theoretical[15] evidence indicating that, in planar systems, they lead to better binding efficiencies than short rigid tethers. The number of monomers per tether is N and the surface coverage of the tethers, i.e., number of grafted polymers per unit area of the channel, is σ. The free end of each tether carries the ligand (L) that can specifically bind to a receptor (R) located on the surface of a protein in solution in order to form a ligand−receptor (LR) bound pair. The chemical equilibrium between the bound and unbound species can be written in the form

$$\mathrm{LR} \rightleftharpoons \mathrm{L} + \mathrm{R} \tag{1}$$

This chemical equilibrium has an intrinsic dissociation constant in bulk solution, which in the calculations presented here is $K^{\theta}_{d} = 10^{-15}$ M. This value corresponds to that of the biotin−avidin system.[33] This dissociation constant is much smaller than the range of protein concentrations explored in this work, therefore the LR pairs are thermodynamically very stable in the bulk solution. Interestingly, as we discuss below, the role of nanoconfinement can result in dramatic changes in the apparent dissociation constant and thus the bound pair may not be thermodynamically stable inside the channel. Each protein is modeled as a spherical particle of radius R_{prot} and charge Q_{prot} with a single receptor located on its surface. Free proteins in solution can freely translate and rotate and participate in ligand−receptor binding with the ligands. In addition to free proteins, the solution contains water molecules and mobile ions (salt anions and cations, protons and hydroxyl ions). Note that the reservoirs are much larger than the nanochannel, thus binding of proteins to the channel walls does not decrease their concentration in solution (i.e., the protein concentration in solution is fixed).

We present here a systematic study of the effect of the geometry of the channel, the ligand-spacer molecule and the proteins on the amount of bound proteins and the conductance response of the channel. To this end we apply a molecular theory that incorporates the size, shape, conformations, charge and charge distribution of the different molecular species and treats the steric, van der Waals and electrostatic interactions explicitly coupled with the ligand−receptor binding equilibrium. The theory is presented in the Methods section. For neutral proteins, we predict that the fraction of the channel blocked by the bound proteins is a nonmonotonic function of the size of the channel, the surface density of the ligands and the length of the polymeric tether. Thus, increasing the surface density of the ligands or decreasing the radius of the channel may decrease the fraction of the channel that is filled by bound proteins. These responses arise from the expulsion of the proteins from the channel due to an increase in the excluded volume interactions. We also discuss the case where the proteins and the channel are charged in order to show that large conductance changes due to protein binding can be achieved when the charge of the channel is opposite to that of the protein.

RESULTS

Structure of the Bound Protein Layer. We start by discussing the structure of the layer of bound proteins for a typical set of parameters: a very long cylindrical channel of radius R = 5 nm and $L \gg R$ (under this condition the system is homogeneous in the z direction due to translational symmetry), tethers of 10 segments and a protein of diameter 2.25 nm, a bulk concentration of 500 nM and zero charge (i.e., at its isoelectric point). The polymer tethers are models for poly(ethylene oxide); i.e., 10 segments corresponds to PEG-440. Figure 2a shows the number density of bound proteins as a function of the distance from the inner wall of the channel (this is the number density of the centers of the proteins). The

DOI: 10.1021/jacs.5b05032
J. Am. Chem. Soc. 2015, 137, 12539−12551

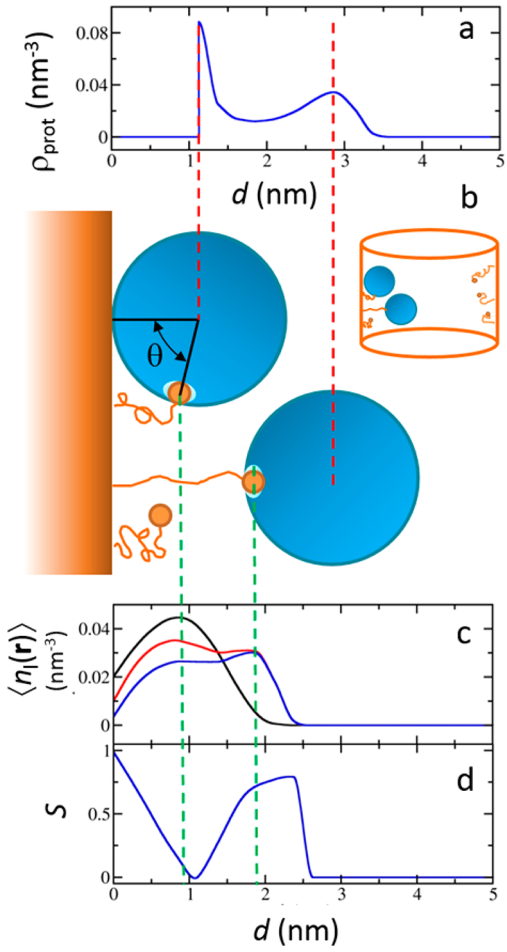

Figure 2. (a) Number density of proteins (determined using the center of the protein) as a function of the distance from the wall of the channel. (b) Schematic representation of the system. The proteins are depicted in the same scale as in panel a. The position of the peaks in the protein density profile (panel a) and the bound-ligand density (panel c) are shown with vertical dashed lines. The inset shows a scheme in a smaller scale than the main figure. (c) Number density of the ligands before (black line) and after (red line) protein binding. The number density of the ligands that are bound to proteins (after protein binding) is shown with the blue line. (d) Orientational order parameter, S, for the proteins bound to the ligands, as defined in eq 2. The angle θ for each bound protein is shown in panel b. The calculations were performed for N (tether length) = 10, σ (surface coverage of ligands) = 0.05 chains·nm^{-2}, R = 5 nm, an infinitely long channel ($L \gg R$) and no protein−protein attractions (χ/χ_C = 0.0).

density of bound proteins shows two peaks, which correspond roughly to two layers of proteins. The density of the first protein layer peaks at 1.125 nm from the surface, which is equal to the radius of the protein and, therefore, the first layer comprises proteins that are in contact with the channel wall. It is favorable to place the first layer of proteins adjacent to the inner wall in order to allow the binding a second protein layer far from the wall. In addition, the cylindrical geometry of the channel implies that the available volume is maximal close to the surface, enabling the binding of a large number of proteins near the wall of the channel. The centers of the proteins in the second layer have a peak density at 2.9 nm from the channel walls (see Figure 2a). This distance is smaller than the sum of the protein radius (1.125 nm) and the length of a fully stretched tether (2.8 nm), therefore, the linkers that bind to proteins in the second layer are not completely stretched. Note also that the distance between the two protein layers (1.7 nm) is smaller than the protein diameter (2.25 nm), which indicates interpenetration between the bound protein layers. Therefore, the two-layer structure is a good description in terms of the distribution of the protein centers but it is important to emphasize that due to interpenetration and positional disorder (i.e., broadness of the peak far from the surface) the structure of the system is not that of two perfectly positioned layers. Note that Figure 2a shows only the density of bound proteins. The density of free proteins (shown in Figure S4 in the Supporting Information) within the channel is much smaller than that of bound proteins, and drops almost to zero near the walls due to steric repulsion with the tethers and bound proteins. Therefore, the free proteins inside the channel do not affect, in any important degree, the conductance of the channel.

Figure 2b shows a cartoon of the organization of the proteins in the same length scale used in panel a. The vertical red dashed lines indicate the position of the centers of the bound proteins. The predicted distribution displayed in Figure 2a shows that the proteins bound in the first layer are highly localized (within less than 0.5 nm) while the second layer is spread over 1.5 nm.

Figure 2c shows the number density of the end-group ligands as a function of the distance from the wall. The ligand density before binding (black line) exhibits only one peak. The formation of bound pairs leads to a second peak in the distribution (red line). In other words, the conformation of the tethers changes in order to facilitate protein binding. The density of ligands that are bound to a receptor (blue line) displays two peaks, which correspond to the two protein layers. The green vertical dashed lines show the position of these peaks in the scheme of Figure 2b. In Figure 2c, the peak closest to the channel wall is broad, which contrasts with the sharp peak observed in the density profile of Figure 2a. This result indicates that the proteins in the first layer have their centers located within a narrow region from d = 1.125 nm to $d \sim 1.5$ nm, but their binding groups are broadly distributed; therefore, there is a broad distribution of protein orientations. On the other hand, the second peak in the density of ligands in Figure 2c is sharper than the first peak, which suggests that the proteins in the second layer are more oriented than those in the first layer, even though they are spatially more delocalized (broad second peak in Figure 2a). The orientation of the protein can be quantified with the orientational order parameter $S(r)$:

$$S(r) = \left\langle \frac{3\cos^2(\theta(r)) - 1}{2} \right\rangle \tag{2}$$

where r is the radial position of the ligand−receptor bond, $\theta(r)$ is the angle between the vector that connects the center of the protein and its binding site and the vector normal to the surface (see Figure 2b) and the brackets denote an ensemble average over all proteins that are bound to a ligand at r. The limits of the order parameter are S = 0 for a completely isotropic orientation and S = 1 or −1/2 when the vector connecting the center of the protein and its binding site is normal or parallel to the surface, respectively.

Figure 2d shows large changes in the order parameter for the bound ligands depending on their distance from the surface of the channel. The ligand−receptor bonds that are in contact with the surface must arise only from proteins oriented perpendicular to the channel wall and, therefore, the plot in

DOI: 10.1021/jacs.5b05032
J. Am. Chem. Soc. 2015, 137, 12539−12551

Figure 2d has an order parameter equal to 1 for $d = 0$. As the distance between the ligand−receptor bond and the surface increases, the number of possible orientations of bound proteins also increases. At the distance where the density of ligands is maximal ($d \sim 1$ nm), protein orientation is almost completely random (order parameter close to zero). It is important to emphasize that the order parameter for a ligand−receptor bond located at d has contributions from proteins with centers at different distances from the surface, thus the random orientation observed for ligand−receptor bonds at $d \sim 1$ nm corresponds to weighted average of all those positions of protein centers, as shown in Figure S2 of the Supporting Information. Figure 2d shows that $S = 0.7$ at the position of the ligands of the second protein layer. The proteins in the second layer are preferentially oriented perpendicularly to the surface in order to optimize binding while reducing protein−protein and protein−tether repulsive interactions. Note that the total number of proteins in a layer is the product of the protein density in that layer by the volume of the cylindrical shell occupied by the layer. This volume decreases as the distance from the surface increases due to the cylindrical geometry of the system, and therefore, the number of bound proteins in the second layer is smaller than those in contact with the channel wall.

The differences in orientational and positional order of the proteins are a manifestation of the interplay between entropy, packing and interactions. The first layer is positionally ordered but orientationally disordered because the proteins locate in the vicinity of the surface. Therefore, the conformational entropy of bound tethers is maximized through a broad distribution of protein orientations. The second layer is positionally disordered but orientationally ordered because the tethers have to stretch to reach the proteins and therefore the proteins preferentially orient perpendicularly to the wall. A rather broad distribution of protein positions grants some conformational disorder to the tethers in order to avoid entropic penalties.

Blocking of Long Nanochannels by Neutral Proteins. We will systematically explore first the case where both the proteins in solution and the channel inner walls are electrically neutral. The use of nanopores and nanochannels in analytical chemistry exploits changes in conductance upon the binding of species in solution into the channel.[5−7] The ability of uncharged proteins to change the conductance of the channel upon binding results from the reduction of available volume in the channel. Namely, the presence of the bound species decreases the cross-sectional area available for ion transport. The change in conductivity is, therefore, controlled by the percentage of the total volume of the channel that is occupied by the bound proteins. We define this percentage of the volume occupied by the bound proteins as $\%F$. Another important indicator is the average fraction of ligands in the channel that are bound to a protein, $\langle f_{\mathrm{bound}} \rangle$, which measures the extent of the ligand−receptor bond-formation reaction. In other words, $\langle f_{\mathrm{bound}} \rangle$ is related to the apparent dissociation constant within the channel (to be defined and quantified later). We calculate $\langle f_{\mathrm{bound}} \rangle$ from

$$\langle f_{\mathrm{bound}} \rangle = \frac{\int\int \langle n_l(\mathbf{r}) \rangle f_b(\mathbf{r}, \mathbf{r}')\, d\mathbf{r}\, d\mathbf{r}'}{\int \langle n_l(\mathbf{r}) \rangle\, d\mathbf{r}} \quad (3)$$

where $\langle n_l(\mathbf{r}) \rangle$ is the number density of ligands at $\mathbf{r}$ and $f_b(\mathbf{r},\mathbf{r}')$ is the fraction of ligands at $\mathbf{r}$ that are bound to proteins with center at $\mathbf{r}'$. Finally, we will define σ_{prot} as the total amount of bound proteins per unit area of the channel, which is given by the product of the fraction of bound ligands multiplied by the surface coverage of ligands, $\sigma_{\mathrm{prot}} = \sigma \cdot \langle f_{\mathrm{bound}} \rangle$.

Figure 3a shows $\%F$ as a function of the channel radius and the surface coverage of the ligands (which are linked to the channel wall by 10-segment tethers). The filling of the channel is maximum for $R \sim 4$ nm and $\sigma \sim 0.06$ chains·nm^{-2}. Interestingly, $\%F$ varies nonmonotonically with σ and R. In principle, a monotonic increase in the number of bound proteins with the surface coverage of the ligands would be expected. However, our theory predicts that $\%F$ can decrease with σ. There are several factors that need to be considered to understand the nonmonotonic dependence shown on Figure 3a. For planar surfaces, theory predicted[15] and later experiments confirmed,[34,35] that the amount of binding in the presence of tether spacers is a nonmonotonic function of the

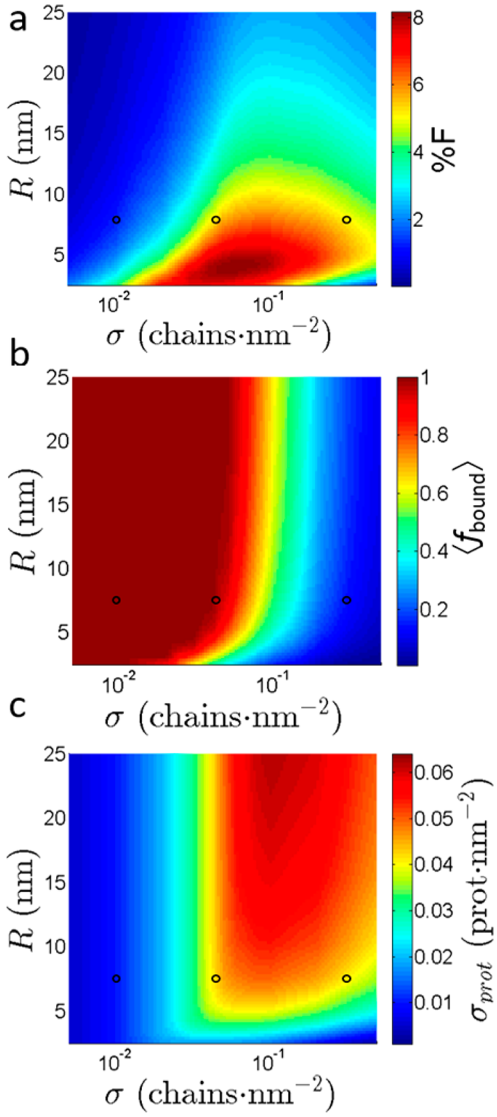

Figure 3. Color maps showing the percentage of the nanochannels volume occupied by bound proteins ($\%F$, panel a), the average fraction of ligands that are bound to the proteins ($\langle f_{\mathrm{bound}} \rangle$, panel b) and the number of protein bound per unit area (σ_{prot}, panel c) as a function of channel radius, R, and surface coverage, σ. Other calculation parameters: $N = 10$, $\chi/\chi_C = 0.0$. Open circles indicate the conditions of the calculations in Figure 4.

DOI: 10.1021/jacs.5b05032
J. Am. Chem. Soc. 2015, 137, 12539−12551

surface density of ligands. In the theoretical calculations[15] it was found that the tethers at low densities allow for the organization of the bound proteins in several layers. However, as the surface coverage increases, the polymers stretch due to lateral osmotic repulsions and do not leave space within the layer for proteins to bind. In the case of narrow channels one also needs to consider the additional complexity that as the distance from the surface increases the available volume decreases. We present next a detailed description of each of these effects.

The decrease of %F with σ for large σ is explained by the decrease of $\langle f_{bound}\rangle$ with σ, see Figure 3b, which results in a nonmonotonic dependence on σ of the bound proteins per unit area, $\sigma_{prot} = \sigma\cdot\langle f_{bound}\rangle$, see Figure 3c. Note also that despite the fact that the bulk concentration of proteins (5×10^{-7} M) is much larger than the dissociation constant ($K^{\theta}_{d} = 10^{-15}$ M), the fraction of bound ligands in Figure 3b can be very small, and close to zero, due to protein−protein and protein−tether steric repulsions and spatial confinement, in particular at small R and large σ. For large R ($R > 25$ nm) the values of $\langle f_{bound}\rangle$ and σ_{prot} in Figure 3a and 3b become independent of R because the length of the linkers is much smaller than the radius of the channel and the system behaves as a planar surface.

In order to understand the competition between binding and confinement that results in the nonmonotonic dependence of %F with the surface coverage, we look at the distribution of the bound proteins and tethers in the system. The cases considered in Figure 4a−c are marked with circles in Figure 3 and correspond to three different surfaces coverages for $R = 7.5$ nm and $N = 10$. For these cases the length of the fully extended tethers (2.8 nm) is shorter than the channel radius. We choose these particular three cases in order to better understand the nonmonotonic binding within the nanochannel (see symbols in Figure 3).

Figure 4a shows the number density of bound proteins as a function of the distance from the channel wall, d. For $\sigma = 0.01$ and 0.05 chains·nm^{-2}, the proteins show a maximum in the bound density at 1.125 nm, which corresponds to proteins in contact with the channel wall. At the lowest surface coverage of tethers (black line) the density of bound proteins decreases monotonically after the maximum. At this low surface coverage all the ligands have bound proteins (left symbol in Figure 3b). For the intermediate surface coverage (red line) the density of proteins shows a second peak at 2.88 nm from the surface, leading to a bilayer structure of the bound proteins. This organization maximizes the number of ligand−receptor bonds, even at the cost of some steric repulsion, as we explained above (Figure 2). Note that the fraction of bound ligands is still close to 1 (middle symbol Figure 3b). The difference between the intermediate and the low surface coverage is that the number of bound proteins is larger and therefore, the best way to accommodate the additional proteins is by stretching some of the tethers.

When the surface coverage of the tethers is increased to 0.5 chains·nm^{-2} (blue line), the tether−tether and tether−protein repulsions increase significantly. The first observation is that there is a significant shift in the position of the first protein density peak toward larger distances from the surface. This is due to the larger volume fraction occupied by the tethers in the vicinity of the surface, as shown in Figure 4c (blue line). The depletion of the proteins from the surface results in the two peaks for the density of bound proteins to be closer than for the more dilute case. In reality this structure optimizes the volume

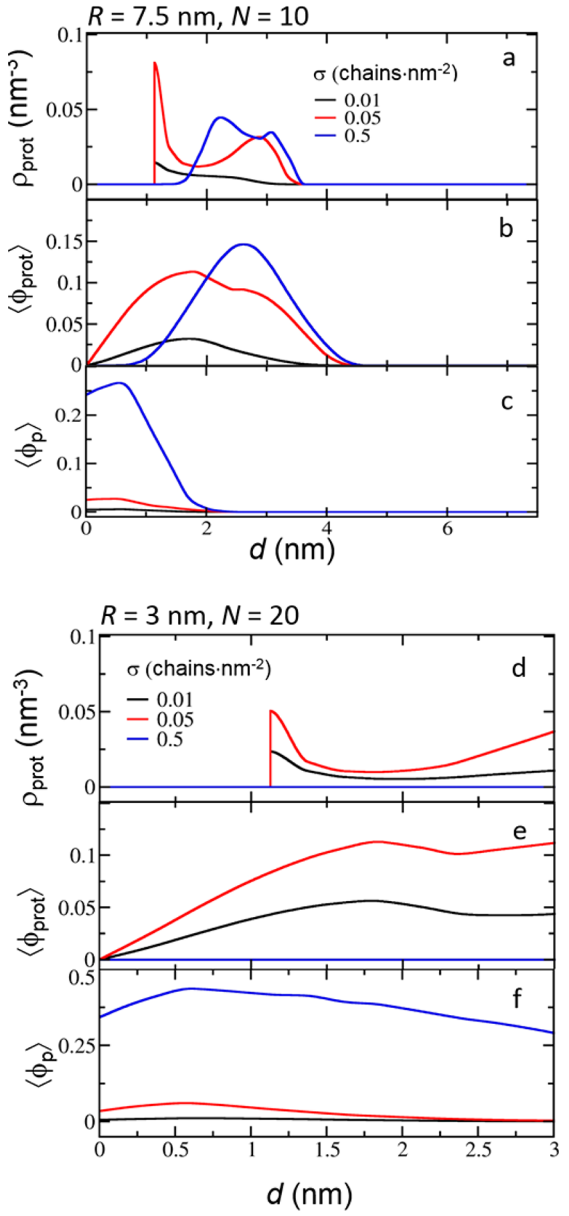

Figure 4. (a,d) Density of bound proteins (determined using the centers of the proteins), (b,e) volume fraction of the bound proteins and (c,f) volume fraction of the polymeric tethers as a function of the distance from the wall of the channel, d, for different surface coverages of the ligands and (a,b,c) $R = 7.5$ nm, $N = 10$ or (d,e,f) $R = 3$ nm, $N = 20$. The calculation parameters used in a, b and c are indicated with open circles in Figure 3.

distribution of both proteins and tethers that are allowed for this given chain length of polymer. Interestingly, the depletion from the surface results in a very small fraction of bound proteins (right symbol Figure 3b) that corresponds to an absolute number of bound proteins similar to that predicted for the case of intermediate surface coverage, even though the surface coverage in that case was five times smaller than in the high surface coverage case. This example demonstrates the very important role that molecular organization within the confined system plays in determining the binding, where more is not necessary better. We next describe the role that the different design parameters play in the interplay between binding optimization and nanoscopic confinement.

DOI: 10.1021/jacs.5b05032
J. Am. Chem. Soc. 2015, 137, 12539−12551

The role of small channel size is presented in Figure 4d, which show that for a nanochannel of R = 3 nm increasing the surface coverage of the tethers from 0.05 chains·nm^{-2} to 0.5 chains·nm^{-2} drives the complete desorption of proteins from the channel. The desorption of the proteins is due to their very large steric repulsions with the polymer tethers, which have a very large volume fraction within the channel, see the blue curve in Figure 4f. The complete exclusion of proteins from a very narrow channel with increasing density of tethers is a confinement effect that arises from the limited volume of the channel. This effect is not observed on planar surfaces or in channels with radii much longer than the length of the tethers.

An interesting prediction in Figure 3 is that %F non-monotonically depends on R. The fact that %F can decrease with decreasing R may be counterintuitive. Particularly, if one assumes the fraction of binding to be constant (a normal assumption made in the literature for strong binders), then decreasing the channel radius would increase the volume fraction of the channel occupied by proteins because the number of available ligands increases linearly with R (i.e., it is proportional to the channel internal area), while the cross-sectional area to be blocked increases as R^2. Therefore, if complete binding occurs, the %F will always increase with decreasing R. However, as R decreases there is also a decrease in the fraction of bound ligands (see Figure 3b for intermediate surface coverages and small radii) because confinement in narrow channels enhances repulsive protein−protein and protein−tether interactions. The decrease in the fraction of ligand−receptor bonds with decreasing R is very large and it is responsible for the nonmonotonic dependence of %F with R.

We next discuss the effect of the length of the tethers, Figure 5. In the case of a planar system, the number of bound proteins is a monotonically increasing function of the length of the linker (see Longo and Szleifer[15]). Long tethers allow the proteins to distribute over a larger range of distances from the surface than short ones, as long as the surface coverage is not too large to completely prevent the partition of some proteins within the polymer layer. Note that this behavior is allowed by the fact that, on planar layers, the volume element as a function of the distance from the surface is constant. On the other hand, Figure 5a shows that %F is a nonmonotonic function of the length of the tether for nanochannels of intermediate radii at intermediate surface coverage of ligands. Figure 5b shows that the nonmonotonic dependence of %F with N is due to a nonmonotonic change of the fraction of bound ligands, $\langle f_{bound} \rangle$. The nonmonotonic dependence of binding efficiency on the length of the tether can be understood by looking at the molecular organization of the bound species and the tethers within the channel. The first thing to consider is that increasing the chain length of the tether at constant surface coverage implies an increase of the volume occupied by the tethers, in particular in the region close to the surface of the channel, see Figure 6c. Thus, the structure of the bound proteins changes significantly with the length of the tether based on two effects. The first is the availability of a larger range of distances where the proteins can bind as the polymer chain length increases. The second, is the reduction in the number of bound proteins close to the surface, as chain length increases, due to the larger steric repulsions imposed by the presence of a larger number of polymer segments there. Figure 6a shows that, as the chain length increases, these effects lead to a decrease in the magnitude of the first protein peak and the appearance of new peaks away from the surface, corresponding to new layers of proteins. These new layers allow increasing the total number of proteins by distributing them within the whole channel, see the volume fraction of the proteins in Figure 6b. Therefore, as the length of the tethers increases, the competition between the increase in the volume that is accessible to accommodate bound

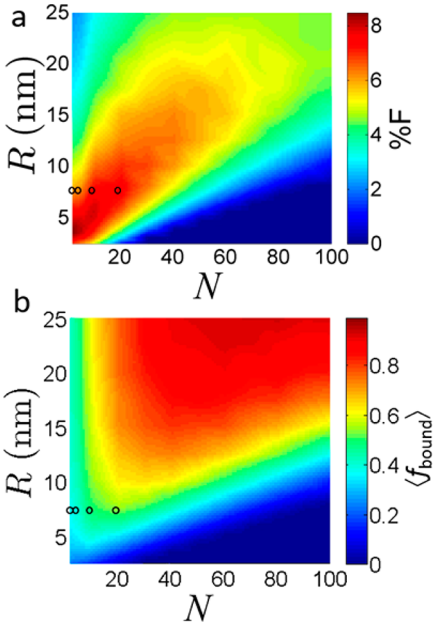

Figure 5. Color map showing the percentage of the channel occupied by bound proteins (%F, panel a) and the average fraction of ligands that are bound to the proteins ($\langle f_{bound} \rangle$, panel b) as a function of channel radius, R, and length of the tethers linking the ligands to the surface of the channel, N. Other calculation parameters: σ = 0.1 chains·nm^{-2}, χ/χ_C = 0.0. Open circles indicate the conditions of the calculations in Figure 6.

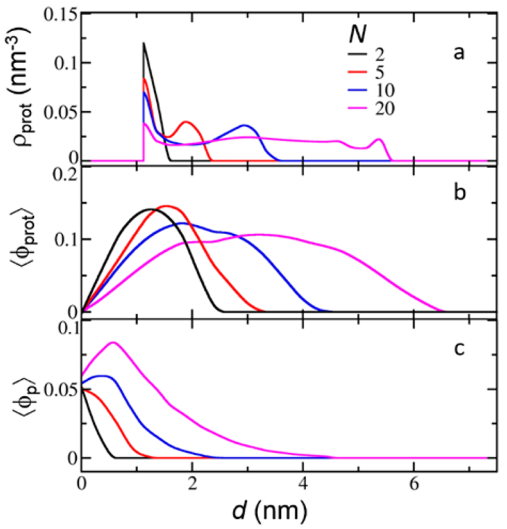

Figure 6. (a) Density of bound proteins (determined using the centers of the proteins) as a function of the distance from the wall of the channel, d, for different lengths of the tethers connecting the ligands to the wall of the nanochannel (N). Other calculation parameters R = 7.5 nm and σ = 0.1 chains·nm^{-2}. (b,c). Volume fraction of the bound proteins (b) and the tethers (c) as a function of the distance from the wall for the same conditions as panel a. The calculation parameters used in the figure are indicated with open circles in Figure 5.

DOI: 10.1021/jacs.5b05032
J. Am. Chem. Soc. 2015, 137, 12539−12551

proteins and the increase in steric repulsions with the tethers results in the maximum in the fraction of bound proteins with chain length shown in Figure 5a.

We finally discuss the role of protein−protein attractive interactions. We model the interaction between proteins using the expression for the van der Waals attractions between two spheres of radius R_{prot}, see Supporting Information. The strength of the interactions is given by the parameter χ, which we normalize by the critical parameter χ_C that is the value of χ required to produce phase separation of the proteins at the working concentration of 500 nM (i.e., χ_C is the value of χ for which the derivative of the chemical potential of the protein with respect to the protein concentration is zero for C_{prot} = 500 nM, see Supporting Information). Figure 7 shows the effect of

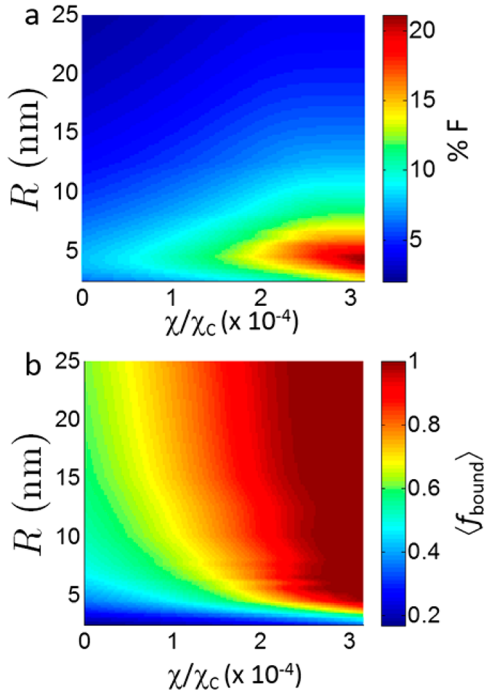

Figure 7. Color map showing the percentage of the channel occupied by bound proteins (%*F*, panel a) and the average fraction of ligands that are bound to the proteins ($\langle f_{bound}\rangle$, panel b) as a function of channel radius, *R*, and strength of the vdW attractions between proteins, χ/χ_C. Other calculation parameters: σ = 0.1 chains·nm^{-2} and N = 10.

χ/χ_C on the fraction of the pore filled by bound protein and the average fraction of bound proteins. As expected, the fraction of bound proteins increases with increasing protein−protein attractions. However, the effect is more important for large radii than for narrow channels. In narrow channels, protein−tether steric repulsions are more important than protein−protein attractive interactions. Thus, the increase of protein−protein attractions produces only a small increase in the fraction of bound protein. The increase of %*F* with χ/χ_C is monotonic and we still observe the nonmonotonic dependence of %*F* with *R* explained above for Figures 3 and 5.

Apparent Dissociation Constant and the Effect of Protein Concentration. A common theme in all the results presented so far is the large shift of the ligand−receptor binding reaction equilibrium that occurs as a result of the confinement in the nanochannels. Therefore, it is important to find appropriate ways to quantify this effect and characterize the chemical equilibrium under confined conditions. For instance, one would like to define an apparent binding constant that can be used later to construct binding isotherms. If we consider the ligand receptor binding as a chemical reaction of the form

$$LR \rightleftharpoons L + R \tag{4}$$

where the ligands are bound to the surface through the tethers, the common approach to describe the binding (adsorption or chemical equilibrium) would be through the Langmuir isotherm, which written in terms of the fraction of bound ligands is

$$\langle f_{bound}\rangle = \frac{C_{prot}}{K_d^{\theta} + C_{prot}} \tag{5}$$

where C_{prot} is the molar concentration of the protein in solution and K_d^{θ} is the dissociation constant. In Figure 8a, we present

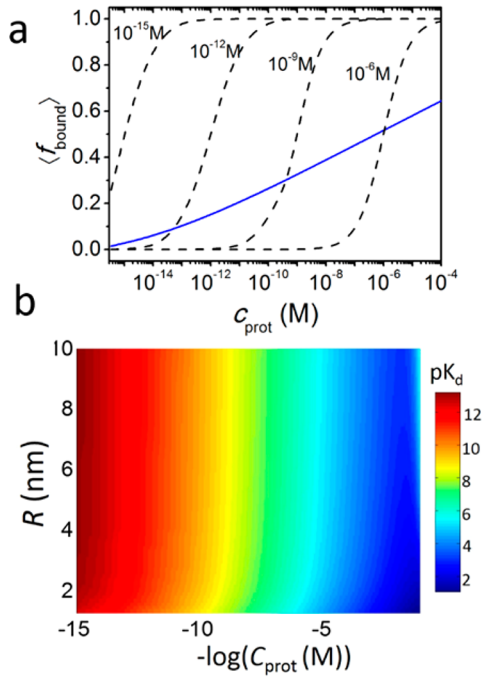

Figure 8. (a) Average fraction of bound ligands as a function of the molar concentration of the proteins in bulk solution (blue line). Calculation parameters: R = 7.5 nm, σ = 0.1 chains·nm^{-2}, N = 10. Dashed lines show the predictions of the Langmuir isotherm eq 5 for different values of the dissociation constant, K_d (the predictions of the molecular theory are for K_d^{θ} = 10^{-15} M). (b) Apparent dissociation constant (determined from eq 6) as a function of R and C_{prot}. Other calculation parameters: σ = 0.1 chains·nm^{-2}, N = 10, χ/χ_C = 0.0.

the Langmuir isotherms for a variety of different dissociation constants K_d^{θ} (dashed lines). The isotherms change from no binding to complete binding for a variation of 2 orders of magnitude of the bulk protein concentration. On the other hand, the predictions of the molecular theory for a typical set of parameters and an intrinsic dissociation constant of 10^{-15} M (blue line) show that a change of 12 orders of magnitude in bulk protein concentration produces only a variation from $\langle f_{bound}\rangle$ = 0 (no binding) to $\langle f_{bound}\rangle$ = 0.6. In other words, the dependence of the fraction of bound proteins predicted by the theory in the confined nanochannel is much weaker than that predicted by a Langmuir isotherm. The main failure in the Langmuir isotherm is that its derivation assumes that the free

DOI: 10.1021/jacs.5b05032
J. Am. Chem. Soc. 2015, 137, 12539−12551

energy cost of binding a protein is independent of the number of bound protein (i.e., independent of $\langle f_{bound} \rangle$) and, therefore, it neglects the effects of confinement and the molecular environment. In the molecular theory, on the other hand, the steric repulsion within the confined channel change with the concentration of bound proteins. Therefore, the molecular theory predicts that the free energy of binding increases significantly as $\langle f_{bound} \rangle$ increases. This effect is mainly due to the increase in the repulsions among bound proteins. Note, therefore, that the interpretation of experimental observations based on the Langmuir isotherm would provide a quantitative and qualitative wrong description of the behavior of these systems.

To better quantify the binding, we show in Figure 8b an apparent dissociation coefficient defined in accordance with eq 5, which we define as

$$K_{d,app} = \frac{(1 - \langle f_{bound} \rangle)}{\langle f_{bound} \rangle} C_{prot} \quad (6)$$

Figure 8b shows that the apparent dissociation constant determined from the predictions of the molecular theory according to eq 6 changes by 15 orders of magnitude for a fixed K^{θ}_{d}. The variation of the apparent dissociation constant over such large range implies that defining an apparent constant as the concentration of reactant where half of the species are bound and assuming that the binding goes from complete to zero in around 2 orders of magnitude of concentration is incorrect and, thus, it needs to be seriously revised.

It is interesting to note that the molecular theory predicts that $\langle f_{bound} \rangle$ increases roughly as the logarithm of the protein concentration (blue solid curve in Figure 8a). We observed a similar trend for calculation conditions different from those in Figure 8 (see Figure S5 in the Supporting Information). The linear relation between $\langle f_{bound} \rangle$ and the logarithm of the protein concentration is, thus, a general trend that arises from the effect of steric interactions on the apparent binding constant. Only a few experimental studies have reported the effect of protein concentration on the conductance of nanochannel sensors for conical nanochannels and a limited range of concentrations spanning 2 orders of magnitude.[6,7] This experimental evidence shows approximately linear relationships between the conductance change and the logarithm of the concentration of the analyte.

Blocking of Short Nanopores. In the previous sections we considered long channels whose lengths are much longer that their radii, ($L \gg R$). Next, we concentrate our attention in nanopores where the length is comparable to the radius. There are several reasons for considering these types of pores. For example, biological nanopores, such as Nuclear Pore Complexes,[36] correspond to this type of geometry. Furthermore, using short pores for conductivity-based determinations may lead to faster response times, since diffusion limitations in long nanochannels can cause long equilibration times.[11] In addition, the results discussed in this section also qualitatively apply to the tips of conical nanochannels.

Figure 9a shows the ratio of the average fraction of bound ligands for a pore of length L to that for an infinitely long channel. The fraction of bound ligands increases as the nanochannel becomes shorter and this effect becomes more pronounced as the length of the tethers increases. In order to understand this effect, we present in Figure 9b the volume fraction of bound proteins in the $r-z$ plane. This plot is similar

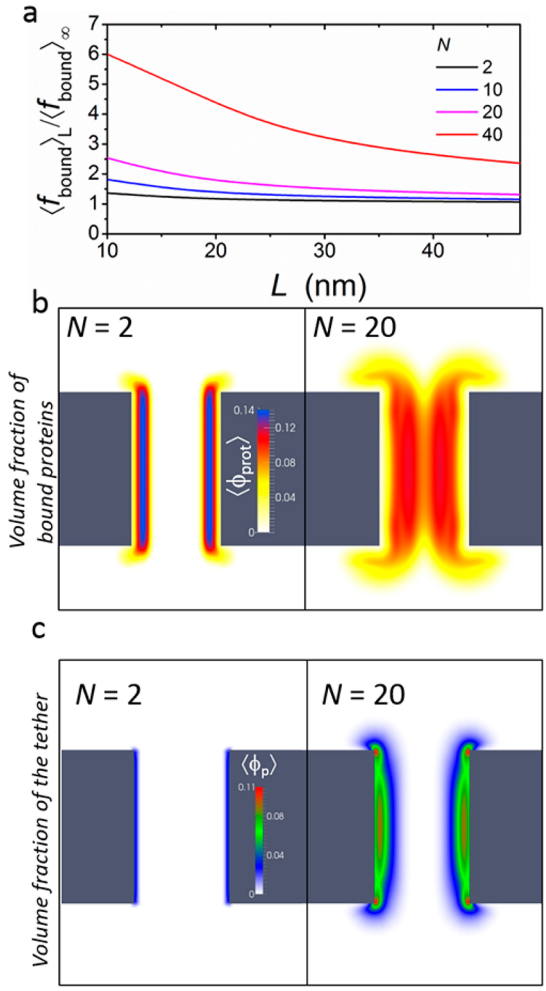

Figure 9. (a) Ratio of the average fraction of bound ligands in a short nanopore of length L, $\langle f_{bound} \rangle_L$, to that in an infinitely long nanochannel, $\langle f_{bound} \rangle_\infty$, as a function of L for tethers of different lengths (N). Other calculation parameters: R = 5 nm, σ = 0.1 chains·nm^{-2}, χ/χ_C = 0.0. (b) Color map for the volume fraction of bound proteins for tether lengths of N = 2 (left panel) and N = 20 (right panel). (c) Color map of the volume fraction of the tethers for the same conditions as panel b. The calculations correspond to a pore of R = 5 nm and L = 16 nm for σ = 0.1 chains·nm^{-2} and χ/χ_C = 0.0.

to those in Figures 4b, 4e and 6b, with the exception that the system is no longer homogeneous in the z direction, therefore we show the density of proteins as a color map that depends now both on r and z. The plot shows that for N = 20 there is a nonzero volume fraction of bound proteins at the entrance of the pore (this is also observed in the plot of bound protein density, see Figure S3 in the Supporting Information). In other words, the ligands attached to long tethers stretch in order to reach the reservoirs on both sides of the membrane. Placing the bound protein in the reservoirs reduces the steric repulsions within the pore, hence the average fraction of bound ligands is larger for short pores than for long channels.

The results of Figure 9 suggest that to maximize the fraction of bound ligands for short nanopores the tethers should be long enough to allow for a large number of bound proteins to be located at the mouths of the pore (i.e., in the reservoirs). However, it is important to emphasize that there is a maximal optimal length, since tethers that are too long reduce the capability of binding as was shown in Figure 5.

DOI: 10.1021/jacs.5b05032
J. Am. Chem. Soc. 2015, 137, 12539−12551

Nanochannel Ionic Conductivity and the Effects of Protein Size and Charge. The results presented in the previous sections correspond to neutral model proteins. Now we show the role of protein size and charge on binding and ionic conductivity. Figure 10a shows a color map of the

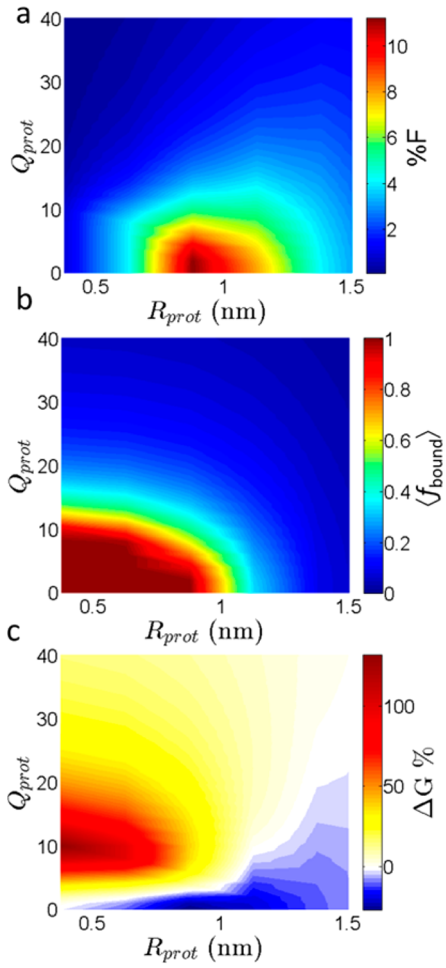

Figure 10. Color maps showing the percentage of the nanochannel occupied by bound proteins (%*F*, panel a), the average fraction of ligands that are bound to the proteins ($\langle f_{bound} \rangle$, panel b) and the change in the conductance of the nanochannel upon protein binding (Δ*G*%, panel c, see eq 8) as a function of the protein radius, R_{prot}, and charge Q_{prot}. The tethers in this calculation were uncharged. Other calculation parameters: R = 4 nm, N = 10, σ = 0.1 chains·nm^{-2}, χ/χ_C = 0.0.

percentage of the volume filled in the channel, %*F*, as a function of the protein charge, Q_{prot} (in units of elemental charge) and radius of the protein, R_{prot} (for a fixed molar concentration of proteins of 500 nM) for a channel of radius R = 4 nm and $L \gg R$. For a fixed charge, %*F* nonmonotonically depends on R_{prot}. Small proteins experience small steric repulsions and bind efficiently (see $\langle f_{bound} \rangle$ in Figure 10b), but they are small, which results in a small %*F*. Large proteins, on the other hand, do not bind effectively due to repulsive steric interactions with other proteins and the polymeric tethers. Therefore, there is an optimal protein size that maximizes %*F*. On the other hand, both %*F* and $\langle f_{bound} \rangle$ always decrease as the protein charge increases due to the increasing electrostatic repulsions among proteins.

For uncharged proteins, Q_{prot} = 0, the change in conductivity upon binding depends on the reduction of the available volume within the channel for the mobile ions. For charged proteins, on the other hand, the change in channel conductivity upon binding depends both on the reduction of the available volume and on the incorporation or release of counterions from the channel. In order to study the contribution of each mechanism to the conductance of the channel, we calculate the conductance using the following expression reported in our previous work:[37]

$$G = \frac{2\pi}{L}\frac{F^2}{RT}\sum_{\substack{i=C,A,\\ H^+,OH^-}} q_i^2 \int_0^R D_i(r)c_i(r)r\ \mathrm{d}r \tag{7}$$

where F is Faraday's constant, q_i is the charge of species i and $c_i(r)$ and $D_i(r)$ are the molar concentration and diffusion coefficient of the species i at a distance r from the center of the channel, respectively. Eq 7 is based on the Goldman constant-field approximation[37−39] and it is valid for very long channels (L > ∼0.5 μm[40]) for which the access resistances are negligible. This equation also implies a continuum description of ion transport, which is valid for channel radii larger than two Debye lengths (R > 1.4 nm for the ionic strength of 0.2 M used here).[41] We assume that the diffusion coefficients in eq 7 are independent of r and equal to those in the bulk. This approximation implies that the changes in conductivity upon protein binding are mainly due to changes in the number of ions within the channel rather than due to changes in their mobility. In a previous work, the predictions of the theory were shown to be in very good agreement with experimental observations for the pH-dependent conductance of polyelectrolyte-modified nanochannels.[37] Therefore, we are confident that this approximation will produce valid predictions in the present case as well. Finally, we assume a very small applied potential, such that the fraction of bound proteins remains equal to that in equilibrium (large applied potentials may affect binding[7,42])

Since we are interested in the relative change in conductance upon binding, rather than in the absolute conductance, we will define Δ*G*% as the percent change in conductance:

$$\Delta G\% = \frac{G - G_0}{G_0} \times 100\% \tag{8}$$

where G_0 and G are the conductances of the system before and after protein binding, respectively. Figure 10c shows a color map of Δ*G*% as a function of Q_{prot} and R_{prot}. For proteins with low charge (small Q_{prot}) or proteins with R_{prot} greater than ∼1 nm, we find Δ*G*% < 0, i.e., a decrease in the channel conductance upon protein binding. Under these conditions (large and uncharged proteins), volume exclusion controls the change in conductance upon protein binding. On the other hand, for charged proteins with R_{prot} smaller than ∼1 nm we observe that Δ*G*% > 0; therefore, the increase of conductance due to the incorporation of the protein counterions to the channel is larger than the decrease of conductance due to the decrease in the available volume. The combined effects of surface charge and volume exclusion can explain the observation that streptavidin binding to biotin ligands within nanochannels may lead either to a decrease[6] or an increase[20] in conductance depending on the properties of the channel and the composition of the solution. In fact, the relative contribution of each mechanism depends also on the ionic

DOI: 10.1021/jacs.5b05032
J. Am. Chem. Soc. 2015, 137, 12539−12551

strength of the measuring solution: Karnik et al.[14] showed that the conductance of a biotin-modified nanochannel increased upon streptavidin binding when the conductance was measured at low ionic strength (and thus the effect of surface charge was more important than volume exclusion), but it decreased at high ionic strength, where volume exclusion is the mechanism dominating the conductance.

In Figure 11, we analyze the case where the tethers connecting the ligands and the walls of the channel have a charge of −|el| per monomer, namely the tethers are polyelectrolytes with charges of opposite sign to that of the proteins. Figure 11a shows that the volume fraction of the channel occupied by bound proteins (%F) is large for proteins of intermediate size ($R \sim 0.7-1.2$ nm) and all charges. In the case of neutral tethers and highly charged proteins (Figure 10), we have shown that protein uptake was prevented by repulsive electrostatic interactions among proteins. In the case of the calculations shown in Figure 11, the electrostatic attraction between tethers and proteins counteracts the electrostatic repulsions among proteins, thus large %F can be obtained for charged proteins.

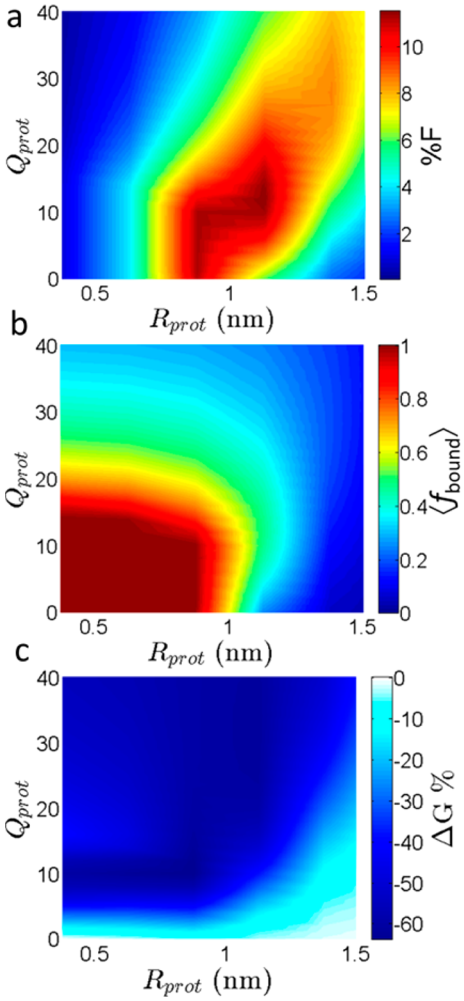

Figure 11. Same as Figure 10, but for polymeric tethers that have a charge of −1 |el| per monomer.

In Figure 11c, we show the change in channel conductance upon protein binding ($\Delta G\%$) for the system of charged tethers. We find that $\Delta G\% < 0$ for all combinations of protein charge and size. This result is in marked contrast to that found for uncharged tethers (Figure 10c), where the conductance increased upon binding of small and highly charged proteins due to the incorporation of counterions into the channel. In the case of tethers with charges of opposite sign than the protein, protein binding leads to a release of the counterions of both the protein and the tether. In other words, the counterions that neutralize the charge of the tethers before protein binding are released as the charges of the protein neutralize the charges of the tethers. This process results in a net decrease in the number of mobile ions inside the channel, therefore the conductance of the channel drops. We suggest that the combination of charge neutralization and volume exclusion can lead to larger and more reliable conductance drops than the volume-exclusion mechanism alone, i.e., compare the maximum conductance drop of $\Delta G\% \sim -60\%$ for a large region of the $Q_{prot}-R_{prot}$ parameter space in Figure 11c (combination of mechanisms) with the maximum value of $\Delta G\% \sim -30\%$ observed for uncharged proteins in Figure 10c (volume exclusion only).

CONCLUSIONS

We presented here the first molecular description of protein binding within nanopores and nanochannels in order to understand the effects of confinement on ligand−receptor binding equilibrium. In Figures 3 and 5, we showed that the fraction of the channel filled by bound neutral proteins is maximal for intermediate surface coverages ($\sigma \sim 0.05$ chains·nm^{-2}), narrow channels ($R \sim 4$ nm) and short linkers ($N \sim 2-5$). However, a more important conclusion is that the optimal length of the tethers increases with R (Figure 5a). A tether shorter than the optimal one will be unable to place bound proteins near the center of the channel, which will result in a decrease of %F. On the other hand, a tether longer than the optimal one will unnecessarily increase the steric repulsions within the channel, which will also reduce protein filling. The calculations in Figure 5 reveal that the fully extended length of the optimal tether should increase by approximately ∼0.9 nm when the channel radius is increased by one nanometer (see Figure S6 in the Supporting Information). In general, it is claimed that channel blocking by proteins is feasible only when the size of the protein and the diameter of the channel are similar,[19] which poses a limitation for sensing since very narrow channels are difficult to prepare. The results in Figure 5 suggest a workaround for this limitation: tethers of appropriate length allow bound proteins to block the whole volume of the channel.

Binding of charged proteins results in changes of conductance that are determined by a combination of the volume-exclusion and the surface-charge mechanisms. The competition between these two mechanisms may give rise to complex behaviors as predicted here and observed experimentally. For example, the binding of streptavidin to immobilized biotin has been reported to decrease the conductance of conical polymer nanochannels,[5,6] to increase that of glass nanopipettes[20] and either to decrease or to increase the conductance of silica parallel-plate nanochannels, depending on the ionic strength of the solution.[14] In this context, an interesting prediction of the theory that may serve to improve the reliability and sensitivity of nanochannel sensors is that when the tethers and the proteins have charges of opposite sign, binding leads to a large drop in conductance of the system (see Figure 11). Siwy and co-workers employed a similar effect to switch the current-rectification properties of

DOI: 10.1021/jacs.5b05032
J. Am. Chem. Soc. 2015, 137, 12539−12551

conical nanopores by binding positively charged avidin to biotin ligands immobilized on negatively charged nanopore tips.[19]

At the fundamental level, we have shown that ligand–receptor binding in nanoconfined environments is qualitative and quantitatively different from the common description used in bulk solution. Namely, the ideal solution approximation does not work due to the importance of intermolecular interactions in the confined pore. Moreover, these interactions cannot be replaced by an effective parameter since they vary in large degrees with all the experimental controllable variables studied. As we have shown, the ligand–receptor binding curve can span more than 10 orders of magnitude in bulk protein concentration, as compared with the 2 orders of magnitude predicted from the commonly used Langmuir isotherm. As a result, the apparent dissociation constant varies more than 10 orders of magnitude with protein concentration; therefore, the use of the concept of dissociation constant itself in nanoconfined environments should be revisited.

The theory provides fundamental understanding of the factors that determine binding and its relationship to ionic conductivity as well as guidelines for the optimal design of nanochannel modifiers. Our theoretical methodology is an enabling tool to study nanopores and nanochannels modified by soft materials as it incorporates molecular information about the components of the system, such as their size, shape, conformations, charge and charge distribution, at a computational cost much smaller than computer simulations. This is a key advantage that allows us to systematically explore the effect of different variables on the molecular organization within the channel and its electrical response. A systematic investigation is important because of the complexity of these systems. For example, we have shown that even for the simplest case of uncharged proteins, the fraction of filled volume within the pore varies nonmonotonically with the channel radius, the surface coverage of the ligands, the length of the tethers and the size of the proteins. It is important, however, to mention the approximations behind our theory. Its mean-field treatment of intermolecular interactions is valid only when each molecule interacts with many other molecules. In the present case, our approximation is expected to breakdown in the limit of very large proteins and short pores, where there may be only a few proteins bound. Therefore, we have limited the current study to small proteins (R_{prot} < 1.5 nm), which yield several proteins per pore; e.g., the short pores in Figure 7b are predicted to contain ~21 proteins for N = 2 and ~34 proteins for N = 20. For the sake of simplicity, we have also neglected some interactions in the present work, such as protein–surface interactions responsible of nonspecific protein adsorption, acid–base equilibrium and hydrogen bonding. While it is possible to include these interactions in the theory[43−45] and to consider in more detail the properties of the protein (such as amino-acid distribution[46] and presence of multiple binding sites[47]), we decided not to consider these additional interactions and molecular details given the very complex behaviors that we observed even in their absence. We expect that, in the future, new experiments will yield detailed data sets and improve the characterization of the nanochannels and that this information will allow us to refine our models by including the relevant interactions for each particular experimental system.

We should finally mention that, in its present formulation, the molecular theory is an equilibrium theory. In some experimental conditions,[7] ligand–receptor binding clearly reaches equilibrium conditions, but in many cases it is not clear whether protein binding is kinetically or thermodynamically controlled. The kinetics of pore blocking can also be used to determine the concentration of the analyte.[5] Thus, in future work we plan to extend our investigations to consider the kinetics of ligand–receptor binding in nanopores, nanochannels and other nanoconfined environments.

METHODS

Our theoretical methodology is based on a previously developed molecular theory,[15,36,37,47] which is formulated here to model ligand–receptor binding equilibria in nanopores and nanochannels. The predictions of the theory have been shown to be in good agreement with experimental observations for ligand–receptor binding on planar surfaces[34] and at liquid–liquid interfaces[47] and the conductance of polyelectrolyte-modified long nanochannels.[37] The molecular theory explicitly accounts for the size, shape, conformation and charge distribution of all molecular species including the ligand, the receptor and the bound pair and it predicts the amount of binding depending on the bulk conditions, e.g., salt and protein concentration.

We formulate the molecular theory by writing down an approximate free energy for the system as a functional of the probability of each conformation of the tether chains, the densities of all mobile species in the system (anions, cations, protons, hydroxyl ions, water molecules and free proteins), the position-dependent fraction of ligands bound to receptors in the proteins and the electrostatic potential. More specifically, the free energy F is given by

$$\begin{aligned}\beta F = & \sum_{\substack{i=A,C,H^+,\\ OH^-,w}} \int \rho_i(\mathbf{r})[\ln(\rho_i(\mathbf{r})v_w) - 1]\, d\mathbf{r} + \\ & + \int\int_{S(\mathbf{r})} \rho_{prot}(\mathbf{r}, \mathbf{r}')[\ln(\rho_{prot}(\mathbf{r}, \mathbf{r}')v_w) - 1 + \beta\mu^0_{prot}]\, d\mathbf{r}'\, d\mathbf{r} \\ & + \sigma \int_P \sum_\alpha P_p(\mathbf{r}, \alpha) \ln(P_p(\mathbf{r}, \alpha))\, d\mathbf{r} \\ & + \int \left[\langle \rho_Q(\mathbf{r})\rangle \beta\psi(\mathbf{r}) - \frac{1}{2}\beta\varepsilon(\nabla\psi(\mathbf{r}))^2\right] d\mathbf{r} \\ & + \int \langle n_l(\mathbf{r})\rangle [f_{unb}(\mathbf{r})(\ln(f_{unb}(\mathbf{r})) + \beta\mu^0_{unbound})]\, d\mathbf{r} \\ & + \int \langle n_l(\mathbf{r})\rangle [\int f_b(\mathbf{r}, \mathbf{r}')(\ln(f_b(\mathbf{r}, \mathbf{r}')) + \beta\mu^0_{bound})\, d\mathbf{r}']\, d\mathbf{r} \\ & + \int d\mathbf{r}_1 \int_{S(\mathbf{r}_1)} d\mathbf{r}_1' \int d\mathbf{r}_2 \int_{S(\mathbf{r}_2)} d\mathbf{r}_2' \left[\frac{\chi}{2} g(|\mathbf{r}_1 - \mathbf{r}_2|)\rho_{prot}(\mathbf{r}_1, \mathbf{r}_1')\rho_{prot}(\mathbf{r}_2, \mathbf{r}_2')\right]\end{aligned} \tag{9}$$

The terms in F account for: the translational entropy of the ions and water molecules (first term), the translational and orientational entropy of the free proteins (second term), the conformational entropy of the tethers (third term), the electrostatic energy (fourth term), the chemical free energy of the ligand–receptor equilibrium (fifth and sixth terms) and the protein–protein vdW attractions (seventh term). In eq 9, $P_P(\mathbf{r},\alpha)$ is the probability of having a tether chain in conformation α grafted at $\mathbf{r}$, $\rho_i(\mathbf{r})$ is the number density of species i at $\mathbf{r}$ (for i = anions, cations, protons, hydroxyl ions and water molecules), $\rho_{prot}(\mathbf{r},\mathbf{r}')$ is the number density of proteins with center at $\mathbf{r}$ and receptor site at $\mathbf{r}'$, $f_{unb}(\mathbf{r})$ is the fraction of ligands at $\mathbf{r}$ that are not bound to proteins, $f_b(\mathbf{r},\mathbf{r}')$ is the fraction of ligands at $\mathbf{r}$ that are bound to proteins with center at $\mathbf{r}'$, $\psi(\mathbf{r})$ is the electrostatic potential at $\mathbf{r}$, $g(r)$ is a function that describes the position-dependent protein–protein attractions and χ sets the strength of these attractions. We describe each term of eq 9 in detail in the Supporting Information.

In order to solve the molecular theory, we find the extremum of a Legendre transform of F that considers constant chemical potentials for all the mobile species with respect to the unknown functions

DOI: 10.1021/jacs.5b05032
J. Am. Chem. Soc. 2015, 137, 12539−12551

$P_P(\mathbf{r},\alpha)$, $\rho_i(\mathbf{r})$, $\rho_{prot}(\mathbf{r},\mathbf{r}')$, $f_{unb}(\mathbf{r})$, $f_b(\mathbf{r},\mathbf{r}')$ and $\psi(\mathbf{r})$. The functional minimization is subjected to the following constraints: (i) global electroneutrality, (ii) packing constraint (modeling the repulsive, excluded volume interactions) at $\mathbf{r}$, i.e., the sum of the volume fractions of all species at $\mathbf{r}$ is one and (iii) the sum of the fractions of bound and unbound receptors at $\mathbf{r}$ is one. These constraints are enforced using Lagrange multipliers.

The functional extremum of the free energy yields analytical expressions for the unknown functions $P_P(\mathbf{r},\alpha)$, $\rho_i(\mathbf{r})$, $\rho_{prot}(\mathbf{r},\mathbf{r}')$, $f_{unb}(\mathbf{r})$, $f_b(\mathbf{r},\mathbf{r}')$ and $\psi(\mathbf{r})$. For example, the density of free proteins is

$$\rho_{prot}(\mathbf{r},\mathbf{r}')v_w = \exp\left(-\int \beta\pi(\mathbf{r}'')v_{prot}(\mathbf{r}'',\mathbf{r}')\right) d\mathbf{r}'' - \int \beta\psi(\mathbf{r}'')q_{prot}(\mathbf{r}'',\mathbf{r})\, d\mathbf{r}'' - \int d\mathbf{r}_2 \int_{s(\mathbf{r}_2)} d\mathbf{r}_2'(\chi g(|\mathbf{r}-\mathbf{r}_2|)\rho_{prot}(\mathbf{r}_2,\mathbf{r}_2')) + \beta\mu_{prot} - \beta\mu^0_{prot} \quad (10)$$

where $\mathbf{r}'$ is a point on the surface of the protein with center at $\mathbf{r}$, v_w is the molecular volume of a water molecule, $\pi(\mathbf{r})$ is the Lagrange multiplier associated with the packing constraint (repulsive interactions), which plays the role of a position-dependent osmotic pressure,[48] $v_{prot}(\mathbf{r}'',\mathbf{r})$ and $q_{prot}(\mathbf{r}'',\mathbf{r})$ are the volume and charge that a protein with center at $\mathbf{r}$ has in the volume between $\mathbf{r}''$ and $\mathbf{r}''+d\mathbf{r}''$ and μ_{prot} and μ^0_{prot} are the chemical potential and the standard chemical potential of the proteins, respectively. Note that the Boltzmann factor in eq 10 has contributions from electrostatic, excluded volume interactions and vdW attractions. In turn, the interaction fields $\pi(\mathbf{r})$ and $\psi(\mathbf{r})$ depend on $\rho_{prot}(\mathbf{r},\mathbf{r}')$ (see Supporting Information), which shows the coupling that exists between the different intermolecular interactions and the distribution of the chemical species in the theory.

The equation for the ligand−receptor equilibrium results from the functional minimization of eq 9 with respect to $f_{unb}(\mathbf{r})$ and $f_b(\mathbf{r},\mathbf{r}')$:

$$K_d = \frac{f_{unb}(\mathbf{r})\rho(\mathbf{r}',\mathbf{r})v_w}{f_b(\mathbf{r},\mathbf{r}')} \quad (11)$$

Eq 11 describes the binding of a protein with its center at $\mathbf{r}'$ and its receptor at $\mathbf{r}$ with a ligand site at $\mathbf{r}$. The dissociation constant in eq 11 has units of (proteins·v_w)/nm^3. We can obtain the commonly used dissociation constant in molar units, K^θ_d,

$$K^\theta_d = \frac{[L][R]}{[LR]} \quad (12)$$

by dividing K^θ_d by v_w·(10^{-24} dm^3/nm^3)·6.02 × 10^{23} proteins/mol. Note that the local fraction of bound ligands at $\mathbf{r}$ in eq 11 depends on the density distribution of proteins, which is a function of $\psi(\mathbf{r})$ and $\pi(\mathbf{r})$, according eq 10, and they are determined by the global minimization of the free energy and therefore depends on the molecular distributions everywhere in the pore. The ligand−receptor binding equilibrium within the channel behave differently from that in the bulk due to the effects of confinement and local molecular environment through the fields $\pi(\mathbf{r})$ and $\psi(\mathbf{r})$.

The expressions for $\psi(\mathbf{r})$, $\rho_i(\mathbf{r})$ and $P_P(\mathbf{r},\alpha)$ that result from finding the functional extremum of the free energy are reported and discussed in the Supporting Information. We cast the final set of integro-differential equations into cylindrical coordinates, discretize it and solve it using numerical methods (see Supporting Information). The input information required by the theory comprises the properties of the tether (chain length, grafting surface density and volume of a segment), the properties of the protein (size, charge and bulk concentration), the value of the dissociation constant for the ligand−receptor equilibrium in the bulk, the properties of the solution (salt concentration and pH) and a large set of random self-avoiding polymer conformations for the tether, which are not allowed to overlap with the walls of the channel. Solving the theory provides us with structural information, such as the position-dependent density of each molecular species, the fraction of bound ligands and the electrostatic potential, as well as with thermodynamic information.

■ ASSOCIATED CONTENT

Supporting Information

The Supporting Information is available free of charge on the ACS Publications website at DOI: 10.1021/jacs.5b05032.

Formulation, discretization and numerical solution of the molecular theory and molecular model. (PDF)

■ AUTHOR INFORMATION

Corresponding Author

*igalsz@northwestern.edu

Notes

The authors declare no competing financial interest.

■ ACKNOWLEDGMENTS

This work was supported by a grant from the NSF, CBET-1403058. MT is a fellow of CONICET. This research was supported in part through the computational resources and staff contributions provided by the Quest high performance computing facility at Northwestern University, which is jointly supported by the Office of the Provost, the Office for Research, and Northwestern University Information Technology.

■ REFERENCES

(1) Bezrukov, S. M.; Vodyanoy, I.; Parsegian, V. A. *Nature* **1994**, *370*, 279.
(2) Dekker, C. *Nat. Nanotechnol.* **2007**, *2*, 209.
(3) Kasianowicz, J. J.; Brandin, E.; Branton, D.; Deamer, D. W. *Proc. Natl. Acad. Sci. U. S. A.* **1996**, *93*, 13770.
(4) Branton, D.; Deamer, D. W.; Marziali, A.; Bayley, H.; Benner, S. A.; Butler, T.; Di Ventra, M.; Garaj, S.; Hibbs, A.; Huang, X.; Jovanovich, S. B.; Krstic, P. S.; Lindsay, S.; Ling, X. S.; Mastrangelo, C. H.; Meller, A.; Oliver, J. S.; Pershin, Y. V.; Ramsey, J. M.; Riehn, R.; Soni, G. V.; Tabard-Cossa, V.; Wanunu, M.; Wiggin, M.; Schloss, J. A. *Nat. Biotechnol.* **2008**, *26*, 1146.
(5) Siwy, Z.; Trofin, L.; Kohli, P.; Baker, L. A.; Trautmann, C.; Martin, C. R. *J. Am. Chem. Soc.* **2005**, *127*, 5000.
(6) Ali, M.; Yameen, B.; Neumann, R.; Ensinger, W.; Knoll, W.; Azzaroni, O. *J. Am. Chem. Soc.* **2008**, *130*, 16351.
(7) Ali, M.; Nasir, S.; Ramirez, P.; Cervera, J.; Mafe, S.; Ensinger, W. *J. Phys. Chem. C* **2013**, *117*, 18234.
(8) Palyulin, V. V.; Ala-Nissila, T.; Metzler, R. *Soft Matter* **2014**, *10*, 9016.
(9) Muthukumar, M. *Polymer Tranlocation*; Taylor & Francis Inc: Bosa Roca, 2011.
(10) Ali, M.; Nasir, S.; Nguyen, Q. H.; Sahoo, J. K.; Tahir, M. N.; Tremel, W.; Ensinger, W. *J. Am. Chem. Soc.* **2011**, *133*, 17307.
(11) Kumar, B. V. V. S. P.; Rao, K. V.; Sampath, S.; George, S. J.; Eswaramoorthy, M. *Angew. Chem.* **2014**, *126*, 13289.
(12) Brunsen, A.; Díaz, C.; Pietrasanta, L. I.; Yameen, B.; Ceolín, M.; Soler-Illia, G. J. A. A.; Azzaroni, O. *Langmuir* **2012**, *28*, 3583.
(13) Ali, M.; Neumann, R.; Ensinger, W. *ACS Nano* **2010**, *4*, 7267.
(14) Karnik, R.; Castelino, K.; Fan, R.; Yang, P.; Majumdar, A. *Nano Lett.* **2005**, *5*, 1638.
(15) Longo, G.; Szleifer, I. *Langmuir* **2005**, *21*, 11342.
(16) Ali, M.; Ramirez, P.; Tahir, M. N.; Mafe, S.; Siwy, Z.; Neumann, R.; Tremel, W.; Ensinger, W. *Nanoscale* **2011**, *3*, 1894.
(17) Sun, Z.; Han, C.; Wen, L.; Tian, D.; Li, H.; Jiang, L. *Chem. Commun.* **2012**, *48*, 3282.
(18) Tian, Y.; Wen, L. P.; Hou, X.; Hou, G. L.; Jiang, L. *ChemPhysChem* **2012**, *13*, 2455.
(19) Vlassiouk, I.; Kozel, T. R.; Siwy, Z. S. *J. Am. Chem. Soc.* **2009**, *131*, 8211.
(20) Umehara, S.; Karhanek, M.; Davis, R. W.; Pourmand, N. *Proc. Natl. Acad. Sci. U. S. A.* **2009**, *106*, 4611.
(21) Fu, Y.; Tokuhisa, H.; Baker, L. A. *Chem. Commun.* **2009**, 4877.

DOI: 10.1021/jacs.5b05032
J. Am. Chem. Soc. 2015, 137, 12539−12551

(22) Jágerszki, G.; Gyurcsányi, R. E.; Höfler, L.; Pretsch, E. *Nano Lett.* **2007**, *7*, 1609.
(23) Wang, X.; Smirnov, S. *ACS Nano* **2009**, *3*, 1004.
(24) Tian, Y.; Hou, X.; Wen, L.; Guo, W.; Song, Y.; Sun, H.; Wang, Y.; Jiang, L.; Zhu, D. *Chem. Commun.* **2010**, *46*, 1682.
(25) Han, C.; Hou, X.; Zhang, H.; Guo, W.; Li, H.; Jiang, L. *J. Am. Chem. Soc.* **2011**, *133*, 7644.
(26) Song, M.; Sun, Z.; Han, C.; Tian, D.; Li, H.; Jiang, L. *Chem. - Eur. J.* **2014**, *20*, 7987.
(27) Zhao, C.; Li, X. S.; Li, L. Y.; Gong, X.; Chang, Y.; Zheng, J. *Chem. Commun.* **2013**, *49*, 9317.
(28) Tian, Y.; Zhang, Z.; Wen, L.; Ma, J.; Zhang, Y.; Liu, W.; Zhai, J.; Jiang, L. *Chem. Commun.* **2013**, *49*, 10679.
(29) Ali, M.; Nasir, S.; Ramirez, P.; Cervera, J.; Mafe, S.; Ensinger, W. *ACS Nano* **2012**, *6*, 9247.
(30) Balamurugan, S.; Obubuafo, A.; McCarley, R. L.; Soper, S. A.; Spivak, D. A. *Anal. Chem.* **2008**, *80*, 9630.
(31) Ravan, H.; Kashanian, S.; Sanadgol, N.; Badoei-Dalfard, A.; Karami, Z. *Anal. Biochem.* **2014**, *444*, 41.
(32) Del Valle, E. M. M.; Galán, M. A. *Ind. Eng. Chem. Res.* **2002**, *41*, 2296.
(33) Green, N. M. *Adv. Protein Chem.* **1975**, *29*, 85.
(34) Zhao, Z.; Matsui, H. *Small* **2007**, *3*, 1390.
(35) Fasoli, E.; Reyes, Y. R.; Guzman, O. M.; Rosado, A.; Cruz, V. R.; Borges, A.; Martinez, E.; Bansal, V. *J. Chromatogr. B: Anal. Technol. Biomed. Life Sci.* **2013**, *930*, 13.
(36) Tagliazucchi, M.; Peleg, O.; Kröger, M.; Rabin, Y.; Szleifer, I. *Proc. Natl. Acad. Sci. U. S. A.* **2013**, *110*, 3363.
(37) Tagliazucchi, M.; Azzaroni, O.; Szleifer, I. *J. Am. Chem. Soc.* **2010**, *132*, 12404.
(38) Goldman, D. E. *J. Gen. Physiol.* **1943**, *27*, 37.
(39) Vlassiouk, I.; Smirnov, S.; Siwy, Z. *Nano Lett.* **2008**, *8*, 1978.
(40) Tagliazucchi, M.; Rabin, Y.; Szleifer, I. *J. Am. Chem. Soc.* **2011**, *133*, 17753.
(41) Corry, B.; Kuyucak, S.; Chung, S. H. *Chem. Phys. Lett.* **2000**, *320*, 35.
(42) Wei, R. S.; Gatterdam, V.; Wieneke, R.; Tampe, R.; Rant, U. *Nat. Nanotechnol.* **2012**, *7*, 257.
(43) Satulovsky, J.; Carignano, M. A.; Szleifer, I. *Proc. Natl. Acad. Sci. U. S. A.* **2000**, *97*, 9037.
(44) Ren, C. L.; Nap, R. J.; Szleifer, I. *J. Phys. Chem. B* **2008**, *112*, 16238.
(45) Tagliazucchi, M.; de la Cruz, M. O.; Szleifer, I. *Proc. Natl. Acad. Sci. U. S. A.* **2010**, *107*, 5300.
(46) Narambuena, C. F.; Longo, G. S.; Szleifer, I. *Soft Matter* **2015**, *11*, 6669.
(47) Ren, C.-l.; Carvajal, D.; Shull, K. R.; Szleifer, I. *Langmuir* **2009**, *25*, 12283.
(48) Nap, R.; Gong, P.; Szleifer, I. *J. Polym. Sci., Part B: Polym. Phys.* **2006**, *44*, 2638.

DOI: 10.1021/jacs.5b05032
J. Am. Chem. Soc. 2015, 137, 12539−12551